

number concentration of cloud droplets can be realistically represented. The aerosol-cloud-radiation interaction is one of the key processes that is missing in many climate models. Every major climate model is adding (if they have not done this already) this interaction [e.g., Morrison and Gettelman, 2008; Gettelman et al., 2008].

[4] Improving mixed-phase cloud parameterizations requires an advanced understanding of cloud and cloud microphysics through carefully planned field studies. In recent years, several major field experiments have been conducted in the Arctic to collect the needed data for model evaluations and improvements. Examples of these field experiments include the Surface Heat Budget of the Arctic Ocean (SHEBA) project [Perovich et al., 1999; Uttal et al., 2002], the First International Satellite Cloud Climatology Project (ISCCP) Regional Experiment (FIRE) Arctic Clouds Experiment (ACE) [Curry et al., 2000], and the Mixed-Phase Arctic Cloud Experiment (M-PACE) [Verlinde et al., 2007]. Detailed in situ observations of Arctic clouds and their microphysical properties have been obtained by using various ground based remote sensors and aircraft in these field campaigns, which provide extremely valuable information to assess and improve model cloud parameterizations.

[5] Direct comparison between climate model simulations and field experiment observations is difficult because climate simulations represent statistics of the atmospheric evolution and are not initialized to any specific time observed during the field campaigns. In order to make a direct model-observation comparison, this study makes use of a tool developed from the Department of Energy (DOE) CCPP-ARM Parameterization Testbed (CAPT) project to initialize climate models with analysis data from Numerical Weather Prediction (NWP) center's data assimilation systems and then evaluate climate models in their short-range weather forecasts using field measurements. Here CCPP and ARM are the DOE Climate Change Prediction Program and Atmospheric Radiation Measurement Program, respectively. The CAPT approach has been proven as a useful way to understand climate model errors and facilitate model parameterization improvements [Phillips et al., 2004; Xie et al., 2004; Boyle et al., 2005; Williamson et al., 2005; Sud et al., 2006; Klein et al., 2006]. By initializing climate models with realistic atmospheric states from NWP analyses for the period where a selected field campaign was conducted under the CAPT framework, the detailed evolution of parameterized variables in short-range weather forecasts can be compared with field experiment data and model deficiencies can be linked directly with specific atmospheric processes observed during the field campaign. Running climate models in NWP mode also allows us to identify specific parameterization deficiencies before the compensation of multiple errors masks the deficiencies, as can occur in model climate simulations.

[6] In this study, two major U.S. climate models, the National Center for Atmospheric Research (NCAR) Community Atmospheric Model version 3 (CAM3) NCAR CAM3 and the NOAA Geophysical Fluid Dynamics Laboratory (GFDL) climate model (AM2), are tested under the CAPT framework against the data collected from the ARM M-PACE field campaign. M-PACE was conducted during the period from 5 to 22 October 2004 near the ARM North

Slope of Alaska site and provided a complete set of measurements for Arctic clouds and their microphysical properties by using millimeter-wave cloud radars (MMCR), micropulse lidars, laser ceilometers, and aircraft [Verlinde et al., 2007]. This study attempts to reveal potential deficiencies related to the cloud and cloud microphysical schemes used in these two climate models by a direct comparison of model results with the in situ and remote sensing data from M-PACE. A new physically based cloud microphysical scheme is also tested in CAM3 to help understand how cloud microphysical processes affect the evolution and phase partitioning of the mixed-phase clouds. The sensitivity of the model results to initial data, model resolution, and cloud ice number concentration is discussed.

[7] The manuscript is organized as follows. Section 2 briefly describes the models and model initialization procedure, with some details given on their cloud and cloud microphysical schemes. A new ice microphysical scheme for CAM3 is also described in this section. Section 3 compares model results with the M-PACE observations. Section 4 shows results from the sensitivity tests. A summary of this study is given in section 5.

2. Models and Model Initialization

2.1. CAM3

[8] CAM3 is the NCAR atmospheric general circulation model (GCM) version 3. CAM3.1 with its finite volume dynamic core at resolution of 2.5° × 2.5° in the horizontal and 26 levels in the vertical is used in this study. There are four model levels below the boundary layer cloud top (850 hPa) observed during M-PACE. Compared to its earlier versions, CAM3 incorporates significant improvements to its physical parameterizations of clouds and radiation. The treatment of cloud microphysics and cloud condensate in CAM3 is based on the prognostic cloud water formulation of Rasch and Kristjánsson [1998] (hereinafter referred to as RK98) with modifications made by Zhang et al. [2003]. RK98 is a single-moment scheme that only predicts the mixing ratio of cloud condensate. The distinction between liquid and ice phase is made as a function of temperature. The fraction of liquid water in the total condensate is defined as:

$$f_l = \begin{cases} 0 & \text{if } T \leq T_{\min} \\ \frac{T - T_{\min}}{T_{\max} - T_{\min}} & \text{if } T_{\min} < T < T_{\max} \\ 1 & \text{if } T \geq T_{\max} \end{cases} \quad (1)$$

where T is temperature, $T_{\min} = -40$ °C, and $T_{\max} = 10$ °C. Further improvements beyond RK98 include separate equations for predicting cloud ice and cloud liquid water, advection of cloud condensate by large-scale circulation, and gravitational settling of cloud ice and liquid particles [Boville et al., 2006]. However, equation (1) is still applied each time step to repartition the cloud liquid water and cloud ice. Cloud fraction in CAM3 is diagnosed for convective clouds based on convective mass flux and for stratiform clouds (C_s) based on relative humidity (RH) outside of the convective cloud according to

$$C_s = \frac{1}{2} \left(\frac{\partial \text{RH}}{\partial p} \right)_{\text{min}} \left(\frac{\partial \text{RH}}{\partial p} \right)_{\text{min}}^2 \quad (2)$$

RH is calculated with respect to water (RH_w) for $T > 0$ C and with respect to ice (RH_i) for $T < 20$ C and is interpolated using RH_w and RH_i between -20 C and 0 C. The threshold relative humidity RH_{min} varies with pressure. Other detailed information about CAM3 is given by Collins et al. [2006].

2.2. AM2

[9] AM2 is the GFDL climate atmospheric model. The model resolution used in this study is 2.0×2.5 in horizontal and 24 levels in vertical (eight levels below 850 mbar). Its cloud microphysical scheme follows Rotstajn [1997] and Rotstajn et al. [2000], in which two separate prognostic equations are used to predict cloud liquid and ice and the liquid/ice partitioning is determined by microphysical processes including the Wegener-Bergeron-Findeisen mechanism, i.e., ice crystals grow at the expense of liquid water [Wegener, 1911; Bergeron, 1935; Findeisen, 1938]. More detailed description about the AM2 cloud microphysical scheme can be found in Ming et al. [2007]. Rotstajn et al. [2000] assumed that saturation vapor pressure in mixed-phase cloud is with respect to liquid. As shown by Rotstajn et al. [2000, equation (5)], the rate of change of cloud ice mixing ratio q_i is

$$\frac{dq_i}{dt} \approx \frac{N_i}{r} \frac{7.8q_i^{1-3} \partial e_{sl}}{r_i^{1-3} \partial A^0} - \frac{e_{sl} b}{B^0 \partial e_{sl}} \quad (3b)$$

Where N_i is the ice number concentration, $q_i = M_i N_i / r$, M_i is the mass of an ice particle, r_i is ice density, e_{sl} and e_{sl} are saturation vapor pressure with respect to ice and liquid, respectively, A^0 and B^0 are terms representing heat conduction and vapor diffusion. See details of this equation in the work by Rotstajn et al. [2000]. The microphysical scheme used in AM2 is a single-moment scheme and its ice number is simply determined by the Meyers et al. [1992] parameterization. Cloud fraction in AM2 is determined by a prognostic cloud fraction scheme developed by Tiedtke [1993]. Further details are available from GFDL Global Atmospheric Model Development Team [2004].

2.3. An Improved Ice Microphysical Scheme for CAM3

[10] A physically based ice microphysical scheme described by Liu et al. [2007a] (LIU07) with slight modifications is also tested in CAM3 to help understand how cloud microphysical processes affect the cloud evolution and cloud ice growth in the mixed-phase clouds. LIU07 was shown to produce a more realistic simulation of the cloud phase structure and the partitioning of condensed water into liquid droplets against observations during the M-PACE than the standard SCAM when tested in the single column mode [Liu et al., 2007b]. LIU07 is a double-moment scheme in which a prognostic equation is used for cloud ice number concentration together with an ice nucleation scheme developed by Liu and Penner [2005]. The liquid and ice mixing ratio is still calculated by the modified RK98 scheme described by Boville et al. [2006] but the liquid mass conversion to ice due to the deposition growth of cloud ice at the expense of liquid water (the Wegener-Bergeron-Findeisen process) is based on the

Rotstajn et al. [2000] scheme. The original Rotstajn et al. [2000] scheme assumes a direct conversion from liquid to ice to maintain liquid water saturation inside in mixed-phase clouds while LIU07 assumes a conversion from water vapor to ice, which results in a smaller conversion rate of liquid to ice in mixed-phase clouds. In this study, we slightly modify LIU07 to allow a direct conversion from liquid to ice as it was assumed in the original Rotstajn et al. [2000] scheme but assume saturation vapor pressure e_w that is weighted by the proportions of ice and liquid water mass for mixed-phase clouds, i.e., $e_w = f_l * e_{sl} + (1 - f_l) * e_{sl}$, where f_l is liquid mass fraction and $0 < f_l < 1$ in mixed phase clouds. So equation (3) used in CAM3LIU becomes:

$$\frac{dq_i}{dt} \approx \frac{N_i}{r} \frac{7.8q_i^{1-3} \partial e_{sl}}{r_i^{1-3} \partial A^0} - \frac{e_{sl} b f_l}{B^0 \partial e_{sl}} \quad (4b)$$

Equation (4) yields a slower growth rate of ice mixing ratio compared to equation (3) because f_l is less than or equal to 1 and $e_{sl} > e_{sl}$. It should be noted that there are debates about relative humidity in mixed-phase clouds. On the basis of in situ data from FIRE-ACE and the Alliance Icing Research Study Projects [Isaac et al., 2001, 2005], Korolev and Isaac [2006] found that water vapor in mixed-phase clouds is close to the saturation over water (i.e., $f_l = 1$) while Fu and Hollars [2004] suggested that the water vapor pressure can be well represented by using the weighting coefficient equal to liquid fraction in the total cloud condensation based on data from the FIRE-ACE project. Korolev and Isaac [2006, p. 2879] explained the different conclusions between these two studies as “a result of a more detailed scheme identifying liquid and ice clouds and a more extensive handling of the corrections in the air temperature and humidity measurements” used by Korolev and Isaac [2006]. It should be noted that both assumptions about saturation vapor pressure in mixed-phase clouds are used in current microphysics parameterizations. For example, Fowler et al. [1996] used a weighted average of the values with respect to ice and liquid water while Rotstajn et al. [2000] assumed vapor saturation with respect to liquid water as described earlier. However, addressing this issue is beyond the scope of the current study.

[11] Another important change to CAM3 by using LIU07 is that the effective radius of cloud ice is now based on the predicted mass and number concentration of ice rather than diagnosed as a function of temperature as in the default model. This will make the computation of model radiation more sensitive to cloud properties and also impact relevant microphysical process rates like sedimentation. The stratiform cloud fraction is calculated using the same RH-based scheme with the same RH_{min} value as that in the default model except that ice supersaturation is allowed in the upper troposphere in the new scheme. As shown later, this can have an impact on simulated cloud fraction.

[12] It is noted that both LIU07 and AM2 use the Rotstajn et al. [2000] scheme for liquid water conversion to ice (Wegener-Bergeron-Findeisen process) in the mixed-phase clouds. Similar to Rotstajn et al. [2000], AM2 assumes that the growth of cloud ice is at the expense of the evaporation of cloud liquid to maintain the liquid water saturation in clouds. As discussed earlier, this could result in

a slightly faster conversion rate of liquid to ice in AM2 than that in the slightly modified LIU07 tested in this study, which assumes that the saturation vapor pressure is weighted by the proportions of ice and liquid water mass for mixed-phase clouds. Another major difference between LIU07 and AM2 is the treatment of cloud ice number. LIU07 uses a prognostic equation to predict the ice number by considering the processes of advection, convective transport, ice nucleation, droplet freezing, microphysical conversion to precipitation, and cloud sublimation. The ice nucleation mechanisms in LIU07 include the homogeneous ice nucleation on sulfate aerosol and heterogeneous immersion nucleation on soot particles in cold clouds with temperature less than -35°C [Liu and Penner, 2005]. In mixed-phase clouds with temperatures between -40°C and -3°C , contact freezing of cloud droplets through the Brownian coagulation with insoluble ice nucleation is considered. Contact ice nuclei are assumed to be mineral dust [Lohmann, 2002]. Deposition/condensation ice nucleation is parameterized assuming the Meyers et al. [1992] (see equation (3) in section 4) function of ice supersaturation. Secondary ice production between -3°C and -8°C is based on Cotton et al. [1986] for Hallet-Mossop multiplication. In contrast, the ice number in AM2 is simply determined by the Meyers et al. [1992] parameterization. Additional discussion on this will be given in section 4. Other differences between LIU07 and AM2 include that LIU07 allows ice supersaturation with respect to ice while the AM2 does not.

2.4. Model Initialization

[13] Both CAM3 and AM2 were initialized from the NASA Data Assimilation Office (DAO) analysis data for M-PACE. More information about the DAO analyses is available at <http://gmao.gsfc.nasa.gov/>. The analysis data were interpolated from the finer-resolution reanalysis grid ($0.5^{\circ} \times 0.5^{\circ}$) to the CAM3 or AM2 grid using the procedures described by Boyle et al. [2005]. These procedures used a slightly different interpolation approach for each of the dynamic state variables, i.e., horizontal winds, temperature, specific humidity and surface pressure, along with careful adjustments to account for the difference in representation of the earth's topography between models. It was judged by comparing with the sounding data collected during the experiment that the DAO analyses reasonably captured the temporal evolution and vertical structure of the observed upper air circulation, temperature, and moisture during M-PACE. This is important since the observed cloud systems during M-PACE are largely controlled by the synoptic-scale circulation [Verlinde et al., 2007].

[14] A series of 3-d forecasts with CAM3 and AM2 are initialized every day at 0000 UT from the DAO analyses for the entire period of M-PACE from 5 to 22 October 2004. The data from hours 12 to 36 of the forecasts were concatenated and averaged onto a 3-h interval are examined in order to reduce the impact of model spin-up that may occur in the first few hours of an integration. In this forecast range, the atmospheric state is still close to the observation so that model errors can be primarily linked to deficiencies in model physics. Results at the model grid point that is closest to the ARM Barrow site (156.4°W , 71.33°N) are compared with the M-PACE observations. The location of

the selected model grid point is (155°W , 72°N) for CAM3 and (156.25°W , 71°N) for AM2. We have examined model results at other nearby grid points and seen some spatial variations in the simulated clouds, but the spatial variations in the simulated clouds among these nearby grid points are much smaller than the differences between model simulations and the observations as shown in next section.

3. Results

3.1. Characteristics of Clouds Observed From M-PACE

[15] Various types of clouds that often occur in the Arctic during its transition season were observed in the M-PACE field experiment. Figure 1a shows the time-pressure cross section of observed frequency of occurrence of clouds at Barrow by integrating measurements from the ARM cloud radar and other sensors using the ARSCL (Active Remotely Sensed Clouds Locations) algorithm [Clothiaux et al., 2000]. These data are originally at 10-s and 45-m time and height intervals. They are averaged to 3-h and 25 hPa intervals to better represent clouds over a large-scale general circulation model (GCM) grid box, which usually represents an area of $200\text{ km} \times 200\text{ km}$. One issue with the ARSCL clouds is that cloud radar tends to underestimate the cloud top heights for high-altitude clouds because it will not be able to detect cloud particles if they sufficiently small. Another issue is that cloud radar detected cloud base can be contaminated with ice precipitation. To reduce this problem, we use the ARM laser ceilometer and micropulse lidar measurements, which are usually insensitive to ice precipitation (if the concentration of precipitation particles is not sufficiently large) or clutter, to determine the cloud base. As indicated by Clothiaux et al. [2000], the laser ceilometers and micropulse lidar can provide quite accurate cloud base measurements.

[16] Even with these uncertainties, the cloud radar and other remote sensors provide extremely valuable information about the vertical distribution of various types of clouds over the ARM Barrow site. During M-PACE, the ARSCL data indicated that Barrow was covered with multilayered stratus clouds in the midlevels and low levels with the cloud top up to 550 hPa for 5–8 October, persistent single-layer boundary layer stratocumulus with the cloud top around 850 hPa during the period from 8 to 14 October, and deep prefrontal and frontal clouds (including cirrus) from 15 to 22 October.

[17] The observed cloud systems were largely controlled by the synoptic-scale circulation affecting that area during M-PACE. As described by Verlinde et al. [2007], for the period from 5 to 15 October, the North Slope of Alaska (NSA) was dominated by a strong surface high-pressure system built over the pack ice to the northeast of the Alaska coast. Associated with the strong surface high, east-northeasterly flow prevailed at low levels. The low-level northeasterly flow combined with a midlevel low-pressure system drifted along the northern Alaska coast generated the complicated multilayer cloud structure over NSA from 5 to 7 October. The single-layer low-level clouds observed from 8 to 15 October originally formed over the ocean adjacent to the Alaskan coast as the low-level east-northeasterly flow brought cold near-surface air from the pack ice

Figure 1. Time-height cross sections of (a) ARSCL cloud frequency and modeled cloud fraction (b) CAM3, (c) AM2, and (d) CAM3LIU at Barrow during M-PACE. The unit is %.

to the warm ocean and then advected to Barrow. Large surface turbulent fluxes are the major driver for the evolution of the boundary layer clouds. During this period, there was a substantial temperature decrease at altitudes below the 665 hPa pressure level and a sharp moisture decrease over the Barrow site. The range of cloud temperature was from 5 C to 20 C, indicating that the cloud condensate was mixed phase. After 14 October, the boundary layer clouds started to disappear as a warm front moved through the area on 15–16 October and a deep ridge moved over the NSA. Southwesterly flow prevailed in the entire troposphere except on late 19 October when there was an abrupt wind direction change from the southwest to the southeast associated with a strong warm frontal passage which brought in deep prefrontal and frontal clouds. Cirrus clouds were seen during this period.

[18] To obtain in situ and remote sensing measurements of microphysical properties of these cloud systems, the ARM millimeter cloud radar, micropulse lidars, laser ceilometers, and two instrumented aircraft were used in the experiment. For the single-layer boundary layer clouds, data collected from both the surface-based remote sensing instruments and the aircraft revealed the presence of a maximum liquid water layer near cloud top and liquid and irregular ice crystals within the cloud layer with precipitating ice beneath the liquid cloud base [McFarquhar et al., 2007]. This result

is consistent with the findings from other arctic field campaigns [Pinto, 1998; Hobbs and Rangno, 1998; Curry et al., 2000]. The multilayered clouds had a more complicated structure than the single-layer clouds. Up to six liquid cloud layers were detected by the ARM narrow-band lidar and the depth of individual liquid cloud layers varied from 50 to 300 m. Combined radar and lidar data indicated the existence of precipitating ice with low ice water content between the layers. These characteristics are similar to those from the in situ measurements by the aircraft. A detailed summary of the observed clouds during M-PACE is given by Verlinde et al. [2007] and McFarquhar et al. [2007]. In the following discussion, we examine how well CAM3 and AM2 capture these observed features in the arctic clouds.

3.2. Model-Simulated Clouds

[19] Figures 1b, 1c, and 1d show the model-produced cloud fraction at Barrow from CAM3, AM2, and the CAM3 with the new ice microphysics described in section 2 (hereafter CAM3LIU), respectively. It should be noted that model clouds represent a fraction of a model grid box occupied by clouds, which is different from the radar and lidar detected frequency of occurrence of clouds as shown in Figure 1a. Cloud fractions in CAM3 and AM2 have to be parameterized in terms of the large-scale variables such as grid mean relative humidity because they cannot be re-

Figure 2. Time series of the total ARSCL cloud frequency and modeled cloud fraction. Black line with dots is for ARSCL, red line is for CAM3, green is for CAMLIU, and blue is for AM2. The unit is %.

solved by CAM3 and AM2 with their current spatial resolutions. There is always a concern about the comparison between the model clouds and the single point radar and lidar measurements. Averaging the ARSCL clouds from the 10-s and 45-m time and height intervals onto the 3-h and 25 hPa intervals improves the representation clouds over a GCM grid box, especially for the highly horizontally advective boundary layer clouds and frontal clouds observed during M-PACE. Nevertheless, it is still difficult to quantitatively compare model clouds with the ARSCL data. So the purpose here is to qualitatively evaluate the model clouds using the available ARM radar and lidar data and demonstrate intermodel differences in their simulated clouds.

[20] Figure 1 shows that all the models are able to qualitatively reproduce the cloud types observed during M-PACE, such as the multilayered clouds from 5 to 8 October, the boundary layer clouds from 8 to 14 October, and the frontal deep high clouds from 15 to 22 October. However, there are considerable differences in detailed structures of the clouds between the observations and the model simulations. For the period 5 to 14 October, the default CAM3 substantially underestimates the observed multilayered and single-layer boundary layer cloud fraction. In contrast, AM2 produces much more midlevel and low-level cloud fraction than CAM3. It is interesting to see that the CAM3 with the new ice microphysics produces more realistic single-layer boundary clouds than the default CAM3 while it generates too many midlevel and high-level clouds. The overestimation of midlevel and high-level clouds is partially related to the scheme's allowance of ice supersaturation. As discussed earlier, CAM3 uses a RH-based cloud scheme to diagnose stratiform cloud fraction (equation (2)) and its RH is determined by a combination of ice and water saturation. Given the same threshold RH_{min} , the new scheme would lead to more cloud fraction than the default CAM3 because of the allowance of ice supersaturation. We have found that the RH in CAM3LIU is often supersaturated with respect to ice in the midlevels and high levels where temperature is usually less than -20°C during M-PACE. One common problem for all the models is that

the modeled cloud top and cloud base are lower than the observed for the period 8–15 October. The averaged cloud [top, base] pressures over this period for ARSCL, CAM3, CAM3LIU, and AM2 are [840, 939], [855, 985], [851, 991], and [865, 1006] (hPa), respectively. This may be partially related to the coarse vertical resolutions used in these models, which cannot well resolve the observed boundary layer structure. For example, CAM3 only has four model levels below 850 hPa, the level of the observed single-layer boundary layer cloud top. For the deep frontal clouds, the models tend to overestimate the clouds at high levels and underestimate them at midlevels and low levels. The problem with the midlevel and low-level clouds is particularly severe for the CAM models. In addition, the model-simulated frontal clouds tend to have a longer lifetime and weaker temporal variability than the observed. This is a common problem for most large-scale models in simulating frontal clouds [e.g., Klein and Jakob, 1999; Zhang et al., 2005; Xie et al., 2005]. The temporal variability in the observed frontal clouds is partially related to subgrid-scale dynamics which cannot be resolved in large-scale models. The difference in temporal variability between the models and observations may also be due to the fact that the ARM observations are from a point whereas the models are grid box averaged.

[21] Figure 2 compares the total cloud fraction from the models and the total cloud frequency from the observations at Barrow. The observed total cloud frequency is calculated from the ARSCL products assuming maximum cloud overlap over a 3-h interval. The observations typically showed a persistent almost 100% cloud cover during the period 5–14 October except on 7–8 and 11 October where the cloud cover decreased slightly. Consistent with earlier discussions, CAM3 considerably underestimates the total cloud cover for this period. This problem is significantly reduced in CAM3LIU when the new physically based ice microphysical scheme is used. AM2 also produces a much better cloud cover than the default CAM3. It is seen that the cloud fraction produced by the default CAM3 shows larger temporal variability than the observations, indicating the inability to produce clouds under the same conditions as nature as the conditions change. In contrast, CAM3LIU and AM2 have 100% cloud cover for most of the period 5–14 October, similar to the observations. For the deep frontal clouds, both CAM3LIU and AM2 largely overestimate the observed cloud fraction while CAM3 generally agrees well with the observation.

[22] Figures 3a–3c show the grid box mean liquid water mixing ratio (LWC) produced from these models. The contour lines in Figure 3 are the model produced temperatures. All the models are able to produce two or more liquid cloud layers for the period 5–8 October even though the fine vertical structures of the observed multilayer clouds as shown by Verlinde et al. [2007] are not well simulated because of the coarse model vertical resolution. In comparison with CAM3LIU, CAM3 predicts similar amount of cloud liquid water for the boundary clouds even though its cloud fraction is much lower. This is partially due to its temperature-dependent liquid/ice partitioning. For the range of temperature -5°C to -20°C , the majority of cloud condensate produced in CAM3 will be liquid. Another noteworthy feature is that CAM3 has much more liquid in

Figure 3. Time-height cross sections of model-produced liquid water mixing ratio (mg/kg). (a) CAM3, (b) AM2, and (c) CAM3LIU. The solid lines are model-simulated temperatures.

the midlevel and upper level clouds than both CAM3LIU and AM2, which leads to a considerable overestimation of the observed liquid water path in CAM3 during these periods. It is noted that AM2-produced clouds contain much less liquid than CAM3LIU for the mixed-phase boundary clouds although they produce comparable cloud fraction and include the Wegener-Bergeron-Findeisen microphysical process. This suggests a faster conversion rate of liquid to ice in AM2 than CAM3LIU, which should be partially related to the differences in specifying the vapor saturation and the cloud ice number concentration between these two models as discussed in section 2.2.

[23] Figure 4 is the same as Figure 3 except for ice water mixing ratio. Since there is no distinction between ice and snow inside the cloud for AM2 (i.e., AM2 ice includes snow inside the cloud) but for CAM3 there is, we add model snowfield to the ice water mixing ratio in CAM3 and CAM3LIU for a better comparison with AM2. For simplicity, we use “ice” to represent the sum of ice and snow in our following discussions. It should be noted that the snow in CAM3 and CAM3LIU has no impact on radiation while the snow inside cloud in AM2 affects model radiation since it is treated as ice. Compared to CAM3 and CAM3LIU, AM2 produces less ice for boundary layer clouds and near the surface partially because of the fact that the snow falling out of clouds is not included in Figure 4b while it produces

significantly larger ice in the strong frontal clouds on 19 October. Generally, CAM3LIU generates more ice than the default CAM3, especially for the boundary layer mixed-phase clouds.

[24] Figures 5a and 5b show the observed and modeled cloud liquid water path (LWP) and cloud ice water path (IWP) at Barrow, respectively. Note that both observed and modeled IWPs include snow component since the observations cannot separate snow from ice. There are two sources for the observed LWP. Both are based on the ARM Microwave Radiometer (MWR) measurements but they are retrieved using different retrieval algorithms. One is based on the algorithm described by Turner et al. [2007] and another one is derived using Wang [2007]. The observed IWP is derived from the ARM cloud radar and lidar measurements [Wang and Sassen, 2002]. The remote sensing retrieved IWP is currently available for the single-layer boundary layer mixed-phase clouds with an estimated error of about 50%. The uncertainty in the LWP retrieved using the algorithm from Turner et al. [2007] is about $15\text{--}25\text{ g m}^{-2}$ for clouds of any liquid water path and it is about 6 g m^{-2} based on the uncertainty estimated in the Wang [2007] retrieved LWP for clouds with LWP up to 40 g m^{-2} (there is no uncertainty estimate for Wang’s data for the M-PACE period where cloud LWP is usually larger than 100 g m^{-2}). It is seen that the LWPs from these two measurements agree

Figure 4. Same as Figure 3 except for ice water mixing ratio (mg/kg).

with each other very well for the period when the radar and lidar retrievals are available. CAM3 reasonably reproduces the observed LWP for the single-layer mixed phase clouds even though its cloud amount is significantly smaller than the observations. This inconsistency between LWP and cloud fraction in CAM3 is due to the fact that CAM3 cloud fraction is determined by its large-scale relative humidity rather than its cloud condensate. One clear problem with the default CAM3 is that it largely overestimates the observed LWP for the midlevel and high-level clouds (e.g., 7, 16, and 18–20 October). This problem is significantly reduced with the use of the new ice microphysical scheme as shown in CAM3LIU, which also predicts a reasonable LWP for the boundary layer clouds. Consistent with earlier discussion, the LWP in AM2 is considerably smaller than the CAM models and the observations for the boundary layer clouds, suggesting the conversion rate of liquid to ice might be too fast in AM2. However, it is surprising to see that the single-layer boundary layer clouds produced by AM2 do not have much ice either. Further sensitivity tests with its microphysical scheme are needed to fully understand this inconsistency. For the frontal clouds occurring during 15–22 October, the IWP simulated by CAM3 and CAM3LIU agree with each other very well while AM2 produces significantly larger IWP than CAM3 for the strong deep frontal clouds on 19 October, which suggests more rapid glaciations occurred in AM2 than the CAM models for the deep frontal clouds.

[25] To better understand the large differences in the simulated cloud fields among these models, we examine the model simulated surface turbulent fluxes, which are largely responsible for driving the evolution of the boundary layer clouds for the period 9–14 October. Since the clouds observed at Barrow originally advected from the ocean adjacent to the Alaskan coast, we examine the model results at an upwind model grid point. The location of this selected upwind model grid point is (152.5°W, 72°N) for CAM3 and CAM3LIU and (153.75°W, 73°N) for AM2. Over 9–14 October, AM2 has slightly larger sensible and latent heat fluxes than CAM3 and CAM3LIU. The average sensible heat flux over this period is 146 W m^{-2} for AM2, 123 W m^{-2} for CAM3, and 129 W m^{-2} for CAM3LIU and the average latent heat flux is 99 W m^{-2} for AM2, 87 W m^{-2} for CAM3, and 85 W m^{-2} for CAM3LIU. The slightly larger heat fluxes in AM2 might partially lead to a larger cloud fraction compared to the default CAM3. However, the large differences shown in the CAM3 and CAM3LIU produced cloud fraction and cloud properties cannot be easily explained by their surface turbulent fluxes, which are very similar for these two models. This suggests that the differences shown in the CAM3 and CAM3LIU simulated clouds are mainly due to the different microphysical parameterizations used in these two models. Over the period, AM2 also produces a slightly larger surface precipitation rates than CAM3 and CAM3LIU. The average surface precipitation rates at Barrow

Figure 5. Time series of the observed and model-produced (a) cloud liquid water path (g/m^2) and (b) ice water path (g/m^2) during M-PACE. The black solid line with dots is from Turner's retrievals, and the plus is from Wang's retrievals. Red lines are for CAM3, green lines are for CAMLIU, and blue lines are for AM2.

are 0.7 mm d^{-1} for AM2, 0.43 mm d^{-1} for CAM3, and 0.42 mm d^{-1} for CAM3LIU.

3.3. Microphysical Properties in the Single-Layer Mixed-Phase Clouds: Model Versus Aircraft Data

[26] During M-PACE, there were four flights conducted on 9–12 October to obtain cloud properties in the single-layer boundary layer mixed-phase clouds. Each flight lasted 1 or 2 h with cloud data collected every 10 s. While these in situ aircraft data provided unique information to understand the microphysical properties in the mixed-phase clouds, it is difficult to use them to quantitatively compare with model results because the mismatches between them. For example, the model outputs are at a much lower temporal and spatial resolution (representing a mean over 3 h and an area of $200 \text{ km} \times 200 \text{ km}$) than the aircraft measurements (10 s, point measurements). So our purpose here is to see if these models can reproduce qualitatively well some important statistical features revealed by the aircraft data. In Figures 6 and 7, a cloud is defined when the total cloud condensate is larger than 0.001 g m^{-3} for both model results and in situ measurements. To improve statistics, the model data used in Figures 6 and 7 are for the entire period from 9 to

14 October when the single layer boundary layer clouds are generated in these models.

[27] Figure 6a displays the liquid fraction (f_l) in the total cloud condensate as a function of height measured by the University of North Dakota (UND) Citation from the four flights conducted on 9–12 October for the single-layer mixed-phase clouds. The 10 s raw aircraft data were processed by McFarquhar et al. [2007]. The cloud altitude is normalized from 0 at liquid cloud base to 1 at cloud top. The aircraft data revealed the dominance of cloud liquid water in the boundary layer mixed-phase clouds with 79% of cases having $f_l > 90\%$. In general, f_l increases with height and is larger than 80% near cloud top. It is important to notice that many data points with low f_l are found in the lower half of the cloud, indicating the presence of significant amounts of ice. The strong liquid layer near cloud top leads to strong cloud top radiative cooling, which may play an important role in maintaining the persistence of mixed-phase boundary layer clouds [e.g., Pinto, 1998].

[28] Figures 6b–6d are the same as Figure 6a except for CAM3, AM2, and CAM3LIU, respectively. The snow component is added to the total cloud condensate when the modeled liquid fraction is calculated in order to be consistent with the aircraft measurements processed by McFarquhar et al. [2007], which include all particles greater than 53 μm . This observed vertical distribution of f_l is clearly not reproduced by CAM3 in which f_l generally decreases with height because of its temperature dependence. The few points with low f_l found at the cloud base in Figure 6b are due to the model-produced snow. In contrast, the observed variation of liquid water fraction with cloud height is reasonably captured by CAM3LIU. AM2 also shows a better agreement with the observations than CAM3. The lack of low f_l points near the cloud base in AM2 is probably due to the fact that the snow falling out of the cloud is not included in the AM2 total cloud condensate when f_l is calculated.

[29] Figure 7a shows the measured f_l as a function of temperature from the same flights as Figure 6a. The measured cloud temperatures during these flights are about between -16°C and -9°C . It is seen that there is no clear relationship between f_l and temperature in the observations. Significant amounts of liquid and ice coexist within this temperature range. It is obvious that any temperature based liquid/ice partitioning schemes will fail to reproduce the observed structure, such as the scheme used in CAM3 (see Figure 7b). Once again, AM2 and CAM3LIU reasonably reproduce the observed variation with temperature of f_l by including the Wegener-Bergeron-Findeisen process (Figures 7c and 7d). This indicates that the Wegener-Bergeron-Findeisen process is critical for the models to correctly capture observed structure of cloud condensate in the mixed-phase clouds.

3.4. Radiation

[30] Clouds have a large impact on surface radiation. However, it is difficult to evaluate model shortwave radiation (SW) with point measurements taken at a station located near the coast (e.g., Barrow). The closest CAM and AM2 model output grid points to the Barrow site cover both ocean and land areas, over which the surface characteristics are very different. For example, there is a very strong

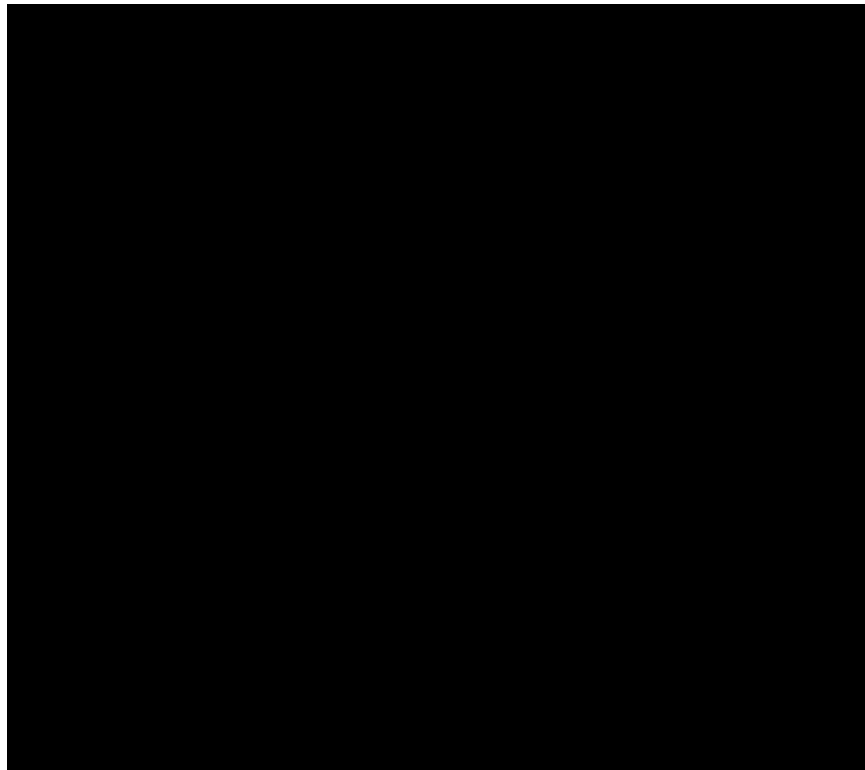


Figure 6. Liquid fraction as a function of cloud height. (a) UND citation data, (b) CAM3, (c) AM2, and (d) CAM3LIU. Different symbols in Figure 6a represent data collected from different flights. Note that the cloud altitude in the figure is normalized from 0 at cloud base to 1 at cloud top.

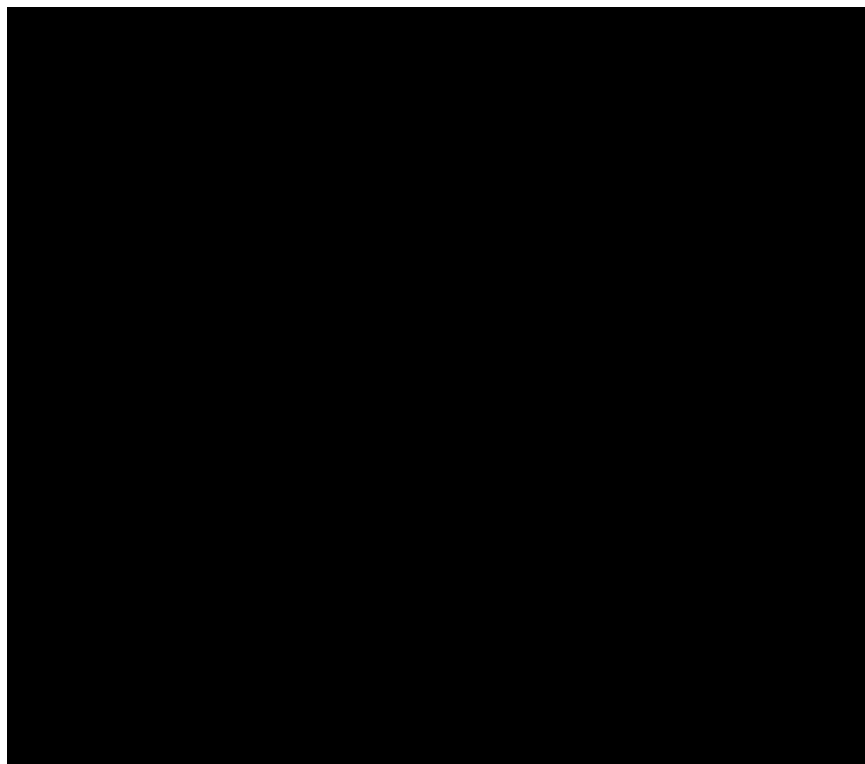


Figure 7. Liquid fraction as a function of temperature. (a) UND citation data, (b) CAM3, (c) AM2, and (d) CAM3LIU. Different symbols in Figure 7a represent data collected from different flights.

Figure 8. Time series of the observed and model-produced (a) surface downwelling longwave radiative fluxes (W/m^2) and (b) TOA outgoing longwave radiative fluxes (W/m^2). Black lines are observations. Red lines are for CAM3, green lines are for CAM3LIU, and blue lines are for AM2.

contrast in the surface albedo between ocean and land. During M-PACE, the ARM Barrow site was covered by snow with the surface albedo in a range of 0.7 to 0.9 [Xie et al., 2006] while its nearby ocean was open water, which had much smaller surface albedo (less than 0.2). The difference in the surface albedo between the models and the observations makes it difficult to interpret model-observation comparison since surface albedo has a large impact on both the surface upward and downward radiation, in addition to clouds. Thus, in this study we will focus our discussion on the surface downward longwave radiation and the top of the atmosphere (TOA) outgoing longwave radiation, which are more related to clouds and less dependent on surface conditions. Moreover, longwave radiative fluxes are the dominant terms in the surface and TOA energy budgets in the cold Arctic season.

[31] Figure 8a displays the observed and modeled downward longwave radiative fluxes (LW) at surface. The observed surface radiation data are obtained from the ARM Solar and Infrared Radiation Station. For the period 5–14 October, the observed surface downward LW shows a rather weak temporal variability due to the presence of persistent low-level clouds. The observed value is significantly underestimated by CAM3, due primarily to its

underestimation of the low-level clouds as shown in Figures 1 and 2. In addition, CAM3 shows much larger temporal variation in the surface downward LW than the observations, consistent with the larger temporal variation in its produced cloud cover (Figure 2). These problems are largely reduced in CAM3LIU, which only slightly overestimates the observations for the period 10–14 October. The overestimation may be related to the lower cloud base altitude in CAM3LIU. AM2 also shows a better simulation of the surface downward LW than CAM3. Its surface downward LW agrees well with the observations for most of the period while it significantly underestimates the observations on days 9, 13, and 14 associated with the problem with its simulated cloud field. The averaged surface downward LW fluxes over the period 5–14 October are 284, 264, 291, and 278 (W/m^2) for the observations, CAM3, CAM3LIU, and AM2, respectively. For the period 15–22 October, all the models generally overestimate the observed surface downward LW, partially because of the longer lifetime for the frontal clouds simulated by these models.

[32] Figure 8b is the same as Figure 8a except for the outgoing longwave radiative fluxes (OLR) at top of the atmosphere. The observed TOA radiative fluxes are from the 1°–1° analysis of the NASA Terra and NOAA 16 satellite measurements. All the models consistently overestimate the observed OLR in the presence of the single-layer boundary layer clouds (9–14 October). This is related to the underestimation of the cloud fraction and cloud liquid water path during this period as discussed earlier. The model underestimation of the low-level cloud top altitude may also contribute to this problem. Compared to CAM3, the overestimation is largely reduced in CAM3LIU. It is seen that CAM3LIU considerably underestimates the observed OLR on day 7 when the multilayered clouds occurred. This is mainly because CAM3LIU clouds extend to much higher altitude (300 hPa) than the observed (~550 hPa) (see Figure 1). For the deep frontal period, the smaller OLR produced by the models on 15–16 October and 17–18 October is consistent with the higher frontal cloud fraction generated by these models compared to the observations.

4. Sensitivity Tests

[33] Several sensitivity tests are conducted to illustrate how sensitive model results are to initial data, model resolution, and cloud ice number concentration. As mentioned earlier, the CAPT approach is to initialize a climate model with the NWP analyses without developing its own data assimilation system. Since the NWP analyses are not perfect and are affected by deficiencies in the model used to produce the analysis, model results may be sensitive to the analyses from different NWP centers. Thus, it is useful to examine if the model behaviors shown in this study are robust and not dependent on a particular analysis. For this purpose, we tested CAM3 and CAM3LIU with the National Center for Environmental Prediction (NCEP) Global Data Assimilation System (GDAS) analysis data (<http://www.emc.ncep.noaa.gov/gmb/gdas/>) for M-PACE. Similar to the DAO analyses, the GDAS analyses also reasonably represent the observed atmosphere for M-PACE but with

slightly smaller biases of generally less than 1 K in temperature and 0.1 g/kg in moisture compared to the errors of less than 1.5 K in temperature and 0.1 g/kg in moisture in the DAO analyses. We found that the forecasts of clouds and cloud microphysical properties with the GDAS data are very similar to those with the DAO analyses as shown in section 3. This indicates that the errors associated with the simulated mixed-phase clouds in CAM3 and the improvements seen in CAM3LIU with the new ice microphysical scheme are rather robust with respect to conditions with initial data.

[34] Another two sensitivity tests were conducted with AM2: AM2N90 is AM2 with a higher horizontal resolution of 1.0° and 1.25° and AM2N90N is the same as AM2N90 but with a modified parameterization of ice number density based on the M-PACE ice nuclei (IN) observations. As described in section 2.2, AM2 uses a parameterization of the Wegener-Bergeron-Findeisen process based upon Rotstain et al. [2000]. The parameterization is based upon the diffusional growth of ice in the presence of liquid drops that maintain the ambient water vapor at liquid water saturation (and thus ice-supersaturation). The rate of change of the ice mixing ratio is proportional to the assumed number density of ice. Since AM2 does not have a prognostic equation for the number density of ice, this is parameterized following Meyers et al. [1992]:

$$N_i = \frac{1}{4} \exp\left[\frac{1}{2} \frac{e_{sl} - e_{si}}{e_{sl}}\right] \quad (5b)$$

Where N_i (L^{-1}) is the ice number concentration, e_{sl} is the saturation vapor pressure of liquid, and e_{si} is the ice saturation vapor pressure. The constant parameters used in equation (5) are empirically determined from midlatitude measurement of ice nuclei (IN) concentrations for the temperature range from -7°C to -20°C, which are generally much higher than Arctic IN concentrations [e.g., Bigg, 1996]. In order to best fit M-PACE observations of ice nuclei, Prenni et al. [2007] modified equation (5) to

$$N_i = \frac{1}{4} \exp\left[\frac{1}{2} \frac{e_{sl} - e_{si}}{e_{sl}}\right] \quad (6b)$$

[35] In the sensitivity study (AM2N90N), equation (6) is used to calculate the ice number density used in the parameterization of the Wegener-Bergeron-Findeisen process. At the typical temperature range of M-PACE clouds (-10°C to -15°C), equation (6) results in a much smaller ice number density of 0.29 L^{-1} as compared to 3.23 L^{-1} from equation (5).

[36] The ice nuclei (IN) concentrations used to obtain equation (6) were obtained from the measurements of a Continuous Flow Diffusion Chamber (CFDC) aboard the Citation aircraft used in M-PACE. The CFDC measurements represent the total number concentration of active IN that have diameters less than 2 μm acting in deposition, condensation, and immersion-freezing modes (without contact freezing). The CFDC IN concentrations are often dramatically different from the ice crystal number concentrations measured by the cloud probes (e.g., one- or two-dimensional cloud probes and the Forward Scattering Spectrometer Probe). For the flights taken on 9–10 October for the single-layer mixed phase clouds, the CFDC mea-

sured IN vary from 0.1 to 1 L^{-1} , which are considerably lower than the ice crystal number concentrations measured by the cloud probes, which generally vary from 0.1 to 10 L^{-1} with an average of 2.8 L^{-1} and a standard deviation of 6.9 L^{-1} [McFarquhar et al., 2007]. Using the CFDC measured IN, current known ice nucleation processes are not able to reproduce the M-PACE observed ice crystal number concentrations, which often exceed the total amount of ice nucleated by at least an order of magnitude [Fridlind et al., 2007]. Fridlind et al. [2007] suggested that this discrepancy could be due to some additional ice initiation mechanisms that are not parameterized in current numerical models and not detected by the CFDC. On the basis of their large-eddy simulations with size resolved microphysics for M-PACE, Fridlind et al. [2007] found that the processes previously hypothesized to explain the discrepancy, such as shattering of drops during freezing and fragmentation during ice-ice collisions, are not able to account for the difference. They further found that the two additional ice initiation processes, formation of ice nuclei from drop evaporation residuals and drop freezing during evaporation, could be strong enough to account for the observed ice crystal number concentration.

[37] Figures 9a displays the simulated cloud fraction from AM2N90 at the model grid point (155.625°W, 71.5°N) closest to Barrow for M-PACE. Compared to the default AM2, AM2N90 produces slightly smaller cloud fraction for the multilayered and single-layer boundary layer clouds. The midlevel clouds from 5 to 8 October are not well captured by AM2N90. As one can expect that the observed temporal variability in deep frontal clouds from 15 to 22 October is better reproduced in AM2N90 since the frontal scale circulations are better resolved with increasing the model horizontal resolution. It is seen that AM2N90-produced clouds contain slightly more liquid water than AM2-simulated, but they are still less than the observations (Figure 10a). The IWP produced by AM2N90 is very similar to that in AM2 (Figure 10b).

[38] Earlier studies have shown that the concentration of ice crystals plays very important role in maintaining mixed-phase clouds in Arctic [Pinto, 1998; Harrington et al., 1999; Jiang et al., 2000]. Using a single-column model coupled to a bulk microphysics parameterization to simulate clouds observed at SHEBA, Morrison et al. [2003] indicated that the model simulated liquid cloud fraction and LWP are very sensitive to uncertainties in the ice number concentration while IWP exhibits comparatively less sensitivity. Consistent with these previous studies, the AM2 simulated clouds and cloud properties also exhibit quite large sensitive to the change in the parameterization of ice number concentration. In general, the smaller ice number density used in AM2N90N leads to a significant increase in both cloud fraction (Figure 9b) and cloud liquid water path for the period 6–15 October (Figure 10a) while there is only a small change in the simulated cloud ice in comparison with AM2N90 (Figure 10b). It is noteworthy that the AM2N90N simulated multilevel and boundary layer clouds are higher in altitude and more close to the observations than AM2N90.

[39] It should be noted that the diagnosed N_i based on the IN observed from the CFDC in the AM2N90N test is much smaller than the M-PACE observed value (0.29 L^{-1} versus

Figure 9. Same as Figure 1 except for (a) AM2N90 and (b) AM2N90N.

2.8 L^{-1}). An overall better performance obtained by AM2N90N compared to AM2N90 that used a N_i closer to the observation (3.23 L^{-1} versus 2.8 L^{-1}) may indicate either the measured ice crystal number concentrations are too large or there are potential problems with the model microphysics parameterizations, i.e., the better results are just for wrong reasons. It is known that the observed ice crystal number concentrations may be slightly overestimated because of ice breakup on aircraft instruments and the CFDC detected IN number concentrations are underestimated by some amount by excluding aerosols larger than 2 mm and contact-mode nucleation. However, these errors cannot fully explain the large discrepancy between these two measurements. As suggested by Fridlind et al. [2007], the large discrepancy could be because some additional ice initiation mechanisms are missing in current parameterizations of ice nucleation processes and are not detected by the CFDC. If we trust the measured ice crystal number concentrations during M-PACE, the worse results from AM2N90 might suggest potential deficiencies with its microphysics scheme. For example, the conversion rate from liquid to ice may be too fast in AM2 because the model significantly underestimates the observed LWP for the mixed-phase clouds if it uses an ice number concentration that is close to the M-PACE observations. Using a lower IN concentration in AM2N90N increases LWP, thus improve the model prediction. The large sensitivity of the model cloud fraction and LWP to uncertainties in the ice number concentrations shown in the AM2N90N test indicates the importance of correctly representing this field in AM2. It also suggests that more accurate measurements of IN and ice crystal number concentrations are required to guide future model microphysics parameterization developments.

[40] Similar to the AM2N90N sensitivity test, we applied the CFDC measured IN (equation (6)) to CAM3LIU to represent deposition/condensation ice nucleation in its ice-phase microphysical scheme. This leads to a much smaller ice number concentration of 0.44 L^{-1} compared to 2.74 L^{-1} from using equation (5) over the flight periods on 9–10 October. Figure 11 shows the simulated cloud fraction

from CAM3LIU with the CFDC measured IN (CAM3-LIUN) for M-PACE. In contrast to the AM2N90N test, the simulated cloud fraction in CAM3LIU is not sensitive to the change in the ice nuclei number concentration. One likely reason is that cloud fraction in CAM3 is not closely linked to its cloud condensate, but rather is more dependent on its large-scale relative humidity as discussed earlier.

Figure 10. Same as Figure 5 except that red line is for AM2, green line is for AM2N90, and blue line is for AM2N90N.

Figure 11. Same as Figure 1 except for CAM3LIUN.

Similar to the AM2N90N test, the smaller ice number concentration in CAM3LIUN results in larger LWP, especially for the single-layer boundary layer mixed-phase clouds observed on 9–14 October (Figure 12a), but the change is not that dramatic as that shown in the AM2N90N test (Figure 10a). For the same period, CAM3LIUN produced smaller IWP than CAM3LIU and the remote sensing retrieved value. Overall, the performance of CAM3LIUN in its simulated clouds is similar to CAM3LIU. This is also different from the results obtained from the AM2N90N test. Reasons for the different responses of CAM3LIU and AM2N90 to the change in the ice number concentrations are complicated because the modeled clouds and cloud microphysical properties also depend on other model processes, including the large-scale dynamic, thermodynamic, and hydrological processes. More in-depth analysis and further sensitivity tests to the parameters used in their microphysical schemes are needed to fully understand the differences in the CAM3LIU and AM2 simulated clouds.

5. Discussion and Summary

[41] We have evaluated the mixed-phase cloud parameterizations used in the two major U.S. climate models, the NCAR CAM3 and GFDL AM2, in short-range forecasts under the DOE CCPP-ARM Parameterization Testbed (CAPT) against the in situ and remote sensing data collected from the ARM M-PACE field experiment over the North Slope of Alaska. We have shown that both models are able to qualitatively capture the various cloud types observed during the M-PACE when they are initialized with realistic atmospheric conditions from the NWP analyses. However, there are significant differences in the simulated cloud fraction and cloud microphysical properties between the two models and between the models and the observations. CAM3 significantly underestimates the observed boundary layer cloud fraction and cannot realistically simulate the variations with temperature and cloud height of liquid water fraction in the total cloud condensate due to an oversimplified cloud microphysical scheme. It also largely overestimates the liquid water path for midlevel and high-level clouds. AM2 reasonably reproduces the observed boundary

layer cloud fraction while its clouds contain much less cloud condensate than CAM3 and the observations. The simulation of the boundary layer mixed-phase clouds and their microphysical properties is considerably improved in CAM3 when a more physically based cloud microphysical scheme is used. The new scheme also leads to an improved simulation of the surface and top of the atmosphere long-wave radiative fluxes. This study has shown that the Wegener-Bergeron-Findeisen process, i.e., the ice crystal growth by vapor deposition at the expense of coexisting liquid water, is important for the models to correctly simulate the characteristics of the observed microphysical properties in mixed-phase clouds.

[42] Sensitivity tests have shown that these results are not sensitive to the initial data produced from two different NWP centers. Increasing model horizontal resolution helps better capture the subgrid-scale features for the Arctic frontal clouds but does not help improve the simulation of the single-layer boundary layer clouds. This might be because the low-resolution climate models could reasonably resolve the single-layer boundary layer clouds, which uniformly covered a large area over NSA and its adjacent oceans during M-PACE. It is shown that AM2 simulated cloud fraction and LWP are sensitive to the change in ice number concentrations used in the Wegener-Bergeron-Findeisen process while CAM3LIU only shows moderate sensitivity in its cloud fields to this change. Fully under-

Figure 12. Same as Figure 5 except that red line is for CAM3LIU and blue line is for CAM3LIUN.

standing the differences between AM2 and CAM3LIU requires more in depth analysis and further sensitivity tests. Reducing uncertainties in the measured IN number concentrations and ice crystals is also important to guide further model microphysics parameterization developments.

[43] It has been shown that the model-produced single-layer boundary layer clouds have lower cloud top and cloud base than the observations. This can have a large impact on the surface and TOA radiation. This problem might be related to the low vertical resolution used in these climate models or deficiencies in the model boundary layer parameterizations. A study to examine the impact of increasing model vertical resolution and/or using an improved boundary layer parameterization on the simulated mixed-phase clouds is ongoing. We will report the results from this study separately.

[44] Acknowledgments. The work reported here was funded by the U.S. Department of Energy Atmospheric Radiation Measurement Program (ARM) and Climate Change Prediction Program (CCPP). The authors would like to thank the two anonymous referees for their valuable comments that helped to clarify and improve the paper. We gratefully thank Greg McFarquhar, David Turner, Zhien Wang, Charles Long, and Patrick Minnis for making the M-PACE field campaign data available for our use. Special thanks go to Renata McCoy for providing the aircraft data in a format that can be easily used for model evaluation. We thank Eugene Clothiaux and Karen Johnson for their help on deriving the cloud fraction from ARSCL products. We thank all the LLNL CAPT team members for their valuable comments on this work. The Climate Data Analysis Tools (CDAT) that were developed in the Program for Climate Model Diagnosis and Intercomparison (PCMDI) were used to perform our analyses. This research was performed under the auspices of the U.S. Department of Energy, Office of Science, Office of Biological and Environmental Research by the University of California, Lawrence Livermore National Laboratory, under contract W-7405-Eng-48. The Pacific Northwest National Laboratory is operated for the DOE by Battelle Memorial Institute under contract DE-AC06-76RLO 1830.

References

- Arctic Climate Impact Assessment (2004), Impacts of a Warming Arctic, 1020 pp., Cambridge Univ. Press, New York.
- Bergeron, T. (1935), On the physics of clouds and precipitation, in *Proces Verbaux de l'Association de Meteorologie*, pp. 156–178, Int. Union of Geod. and Geophys., Karlsruhe, Germany.
- Bigg, E. K. (1996), Ice forming nuclei in the high Arctic, *Tellus*, 48, 223–233.
- Boville, B. A., P. J. Rasch, J. J. Hack, and J. R. McCar (2006), Representation of clouds and precipitation processes in the Community Atmosphere Model Version 3 (CAM3), *J. Clim.*, 19, 2184–2198.
- Boyle, J. S., et al. (2005), Diagnosis of Community Atmospheric Model 2 (CAM2) in numerical weather forecast configuration at the Atmospheric Radiation Measurement sites, *J. Geophys. Res.*, 110, D15S15, doi:10.1029/2004JD005042.
- Clothiaux, E. E., et al. (2000), Objective determination of cloud heights and radar reflectivities using a combination of active remote sensors at the ARM CART sites, *J. Appl. Meteorol.*, 39, 645–665.
- Collins, W. D., et al. (2006), The formulation and atmospheric simulation of the Community Atmosphere Model Version 3 (CAM3), *J. Clim.*, 19, 2144–2161.
- Cotton, W. R., G. J. Tripoli, R. M. Rauber, and E. A. Mulvihill (1986), Numerical simulation of the effects of varying ice crystal nucleation rates and aggregation processes on orographic snowfall, *J. Clim. Appl. Meteorol.*, 25, 1658–1680.
- Curry, J. A., W. B. Rossow, D. Randall, and J. L. Schramm (1996), Overview of Arctic cloud and radiation characteristics, *J. Clim.*, 9, 1731–1764.
- Curry, J. A., et al. (2000), FIRE Arctic Clouds Experiment. Overview of Arctic cloud and radiation properties, *Bull. Am. Meteorol. Soc.*, 81, 5–29.
- Findeisen, W. (1938), Kolloid-meteorologische Vorgänge bei Neiderschlags-bildung, *Meteorol. Z.*, 55, 121–133.
- Fridlind, A. M., A. S. Ackerman, G. McFarquhar, G. Zhang, M. R. Poellot, P. J. DeMott, A. J. Prenni, and A. J. Heymsfield (2007), Ice properties of single-layer stratocumulus during the Mixed-Phase Arctic Cloud Experiment: 2. Model results, *J. Geophys. Res.*, 112, D24202, doi:10.1029/2007JD008646.
- Fowler, L., D. D. A. Randall, and S. A. Rutledge (1996), Liquid and ice cloud microphysics in the CSU general circulation model. Part I: Model description and simulated microphysical processes, *J. Clim.*, 9, 489–529.
- Fu, Q., and S. Hollars (2004), Testing mixed-phase cloud water vapor parameterizations with SHEBA/FIRE-ACE observations, *J. Atmos. Sci.*, 61, 2083–2091.
- Gettelman, A., H. Morrison, and S. J. Ghan (2008), A new two-moment bulk stratiform cloud microphysics scheme in the Community Atmosphere Model (CAM3), part II: Single-column and global results, *J. Clim.*, in press.
- GFDL Global Atmospheric Model Development Team (2004), The new GFDL global atmosphere and land model AM2-LM2: Evaluation with prescribed SST simulations, *J. Clim.*, 17, 4641–4673.
- Gregory, D., and D. Morris (1996), The sensitivity of climate simulations to the specification of mixed phase clouds, *Clim. Dyn.*, 12, 641–651.
- Harrington, J. Y., T. Reisen, W. R. Cotton, and S. M. Kreidenweis (1999), Cloud resolving simulations of Arctic stratus. Part II: Transition-season clouds, *Atmos. Res.*, 51, 45–75.
- Hobbs, P. V., and A. L. Rangno (1998), Microstructures of low and middle-level clouds over the Beaufort sea, *Q. J. R. Meteorol. Soc.*, 124, 2035–2071.
- Isaac, G. A., et al. (2001), Recent Canadian research on aircraft in-flight icing, *Can. Aeronaut. Space J.*, 47, 213–221.
- Isaac, G. A., et al. (2005), First results from the Alliance Icing Research Study II, preprints, AIAA 43d Aerospace Science Meeting and Exhibit, Am. Inst. of Aeronaut. and Astron., Reno, Nev.
- Jiang, H., W. R. Cotton, J. O. Pinto, J. A. Curry, and M. J. Weissbluth (2000), Cloud resolving simulations of mixed-phase Arctic stratus observed during BASE: Sensitivity to concentration of ice crystals and large-scale heat and moisture advection, *J. Atmos. Sci.*, 57, 2105–2117.
- Klein, S. A., and C. Jakob (1999), Validation and sensitivities of frontal clouds simulated by the ECMWF model, *Mon. Weather Rev.*, 127, 2514–2531.
- Klein, S. A., et al. (2006), Diagnosis of the summertime warm and dry bias over the U.S. Southern Great Plains in the GFDL climate model using a weather forecasting approach, *Geophys. Res. Lett.*, 33, L18805, doi:10.1029/2006GL027567.
- Korolev, A., and G. A. Isaac (2006), Relative humidity in liquid, mixed-phase, and ice clouds, Validation and sensitivities of frontal clouds simulated by the ECMWF model, *J. Atmos. Sci.*, 63, 2865–2880.
- Li, Z.-X., and H. Le Treut (1992), Cloud-radiation feedbacks in a general circulation model and their dependence on cloud modeling assumptions, *Clim. Dyn.*, 7, 133–139.
- Liu, X., and J. E. Penner (2005), Ice nucleation parameterization for global models, *Meteorol. Z.*, 14(4), 499–514.
- Liu, X., J. E. Penner, S. Ghan, and M. Wang (2007a), Inclusion of ice microphysics in the NCAR Community Atmospheric Model version 3 (CAM3), *J. Clim.*, 20, 4526–4547.
- Liu, X., S. Xie, and S. J. Ghan (2007b), Evaluation of a new mixed-phase cloud microphysics parameterization with CAM3 single-column model and M-PACE observations, *Geophys. Res. Lett.*, 34, L23712, doi:10.1029/2007GL031446.
- Lohmann, U. (2002), Possible aerosol effects on ice clouds via contact nucleation, *J. Atmos. Sci.*, 59, 647–656.
- McFarquhar, G. M., G. Zhang, M. R. Poellot, G. L. Kok, R. McCoy, T. Tooman, A. Fridlind, and A. J. Heymsfield (2007), Ice properties of single-layer stratocumulus during the Mixed-Phase Arctic Cloud Experiment: 1. Observations, *J. Geophys. Res.*, 112, D24201, doi:10.1029/2007JD008633.
- Meyers, M. P., P. J. DeMott, and W. R. Cotton (1992), New primary ice nucleation parameterizations in an explicit cloud model, *J. Appl. Meteorol.*, 31, 708–721.
- Ming, Y., et al. (2007), Modeling the interactions between aerosols and liquid water clouds with a self-consistent cloud scheme in a general circulation model, *J. Atmos. Sci.*, 64, 1189–1209.
- Morrison, H., and A. Gettelman (2008), A new two-moment bulk stratiform cloud microphysics scheme in the Community Atmosphere Model (CAM3), part I: Description and numerical tests, *J. Clim.*, in press.
- Morrison, H., M. D. Shupe, and J. A. Curry (2003), Modeling clouds observed at SHEBA using a bulk microphysics parameterization implemented into a single-column model, *J. Geophys. Res.*, 108(D8), 4255, doi:10.1029/2002JD002229.
- Perovich, D. K., et al. (1999), Year on ice gives climate insights, *Eos Trans. AGU*, 80, 481.
- Phillips, T. J., et al. (2004), Evaluating parameterizations in GCMs: Climate simulation meets weather prediction, *Bull. Am. Meteorol. Soc.*, 85, 1903–1915.
- Pinto, J. O. (1998), Autumnal mixed-phase cloudy boundary layers in the Arctic, *J. Atmos. Sci.*, 55, 2016–2038.

- Prenni, A. J., et al. (2007), Can ice-nucleating aerosols affect Arctic seasonal climate?, *Bull. Am. Meteorol. Soc.*, **88**, 541–550.
- Rasch, P. J., and J. E. Kristjánsson (1998), A comparison of the CCM3 model climate using diagnosed and predicted condensate parameterizations, *J. Clim.*, **11**, 1587–1614.
- Rotstayn, L. D. (1997), A physical based scheme for the treatment of stratiform clouds and precipitation in large-scale models. I: Description and evaluation of the microphysical processes, *Q. J. R. Meteorol. Soc.*, **123**, 1227–1282.
- Rotstayn, L. D., B. F. Ryan, and J. J. Katzfey (2000), A scheme for calculation of the liquid fraction in mixed-phase stratiform clouds in large-scale models, *Mon. Weather Rev.*, **128**, 1070–1088.
- Sud, Y. C., D. M. Mocko, and S. J. Lin (2006), Performance of two cloud-radiation parameterization schemes in the finite volume general circulation model for anomalously wet May and June 2003 over the continental United States and Amazonia, *J. Geophys. Res.*, **111**, D06201, doi:10.1029/2005JD006246.
- Tiedtke, M. (1993), Representation of clouds in large-scale models, *Mon. Weather Rev.*, **121**, 3040–3061.
- Turner, D. D., S. A. Clough, J. C. Liljegren, E. E. Clothiaux, K. Cady-Pereira, and K. L. Gaustad (2007), Retrieving liquid water path and precipitable water vapor from Atmospheric Radiation Measurement (ARM) microwave radiometers, *IEEE Trans. Geosci. Remote Sens.*, **45**, 3680–3690.
- Uttal, T., et al. (2002), Surface heat budget of the Arctic Ocean, *Bull. Am. Meteorol. Soc.*, **83**, 255–275.
- Vavrus, S. (2004), The impact of cloud feedbacks on Arctic climate under greenhouse forcing, *J. Clim.*, **17**, 603–615.
- Verlinde, J., et al. (2007), The Mixed-Phase Arctic Cloud Experiment, *Bull. Am. Meteorol. Soc.*, **88**, 205–221.
- Wang, Z. (2007), Refined two-channel microwave radiometer liquid water path retrieval at cold regions by using multiple-sensor measurements, *IEEE Geosci. Remote Sens. Lett.*, **4**, 591–595.
- Wang, Z., and K. Sassen (2002), Cirrus cloud microphysical property retrieval using lidar and radar measurements. Part II: Midlatitude cirrus microphysical and radiative properties, *J. Atmos. Sci.*, **59**, 2291–2302.
- Wegener, A. (1911), *Thermodynamik der Atmosphäre*, 331 pp., J. A. Barth, Leipzig, Germany.
- Williamson, D. L., et al. (2005), Moisture and temperature balances at the Atmospheric Radiation Measurement Southern Great Plains Site in forecasts with the Community Atmosphere Model (CAM2), *J. Geophys. Res.*, **110**, D15S16, doi:10.1029/2004JD005109.
- Xie, S., M. Zhang, J. S. Boyle, R. T. Cederwall, G. L. Potter, and W. Lin (2004), Impact of a revised convective triggering mechanism on Community Atmosphere Model, Version 2, simulations: Results from short-range weather forecasts, *J. Geophys. Res.*, **109**, D14102, doi:10.1029/2004JD004692.
- Xie, S. C., et al. (2005), Simulations of midlatitude frontal clouds by single-column and cloud-resolving models during the Atmospheric Radiation Measurement March 2000 cloud intensive operational period, *J. Geophys. Res.*, **110**, D15S03, doi:10.1029/2004JD005119.
- Xie, S., S. A. Klein, J. J. Yio, A. C. M. Beljaars, C. N. Long, and M. Zhang (2006), An assessment of ECMWF analyses and model forecasts over the North Slope of Alaska using observations from the ARM Mixed-Phase Arctic Cloud Experiment, *J. Geophys. Res.*, **111**, D05107, doi:10.1029/2005JD006509.
- Zhang, M., W. Lin, C. S. Bretherton, J. J. Hack, and P. J. Rasch (2003), A modified formulation of fractional stratiform condensation rate in the NCAR Community Atmospheric Model (CAM2), *J. Geophys. Res.*, **108**(D1), 4035, doi:10.1029/2002JD002523.
- Zhang, M. H., et al. (2005), Comparing clouds and their seasonal variations in 10 atmospheric general circulation models with satellite measurements, *J. Geophys. Res.*, **110**, D15S01, doi:10.1029/2005JD005923.
- J. Boyle, S. A. Klein, and S. Xie, Lawrence Livermore National Laboratory, Livermore, CA 94551, USA.
- S. Ghan and X. Liu, Pacific Northwest National Laboratory, Richland, WA 99352, USA.